nature chemistry

SUPPLEMENTARY INFORMATION

DOI: 10.1038/NCHEM.1434

Label-free measuring and mapping of binding kinetics of membrane proteins in single living cells

Wei Wang[1], Yunze Yang[1], Shaopeng Wang[1], Vinay J Nagaraj[1], Qiang Liu[2], Jie Wu[2] and Nongjian Tao[*1,3,4]

[1]Center for Bioelectronics and Biosensors, Biodesign Institute, Arizona State University, Tempe, AZ 85287, USA

[2]Division of Neurology, Barrow Neurological Institute, St. Joseph's Hospital and Medical Center, Phoenix, AZ 85013, USA

[3]Department of Electrical Engineering, Arizona State University, Tempe, AZ 85287, USA

[4]State Key Laboratory of Analytical Chemistry for Life Science, School of Chemistry and Chemical Engineering, Nanjing University, Nanjing 210093, PR China

*Corresponding authors: njtao@asu.edu

1. Flow system....3

2. Glycoprotein-lectin interaction....4

2.1 SPRM movie and corresponding snapshots....4

2.2 The inhibition effect of N-acetyl glucosamine (GlcNAc)....5

2.3 Repeatable regeneration of cell surface....6

2.4 Interaction between WGA and poly-L-lysine....6

2.5 Multiple cell responses....7

2.6 Influence of cell fixation on the binding kinetics....8

2.7 Flow rate.....9
2.8 Long recording time.....10
2.9 Receptor density estimation.....11
2.10 Association and dissociation constant maps.....11
2.11 Equilibrium dissociation constant analysis.....12
2.12 Spatial variation of dissociation rate constant (kd) in Fig. 3c.....13
2.13 Sensitivity of the present SPRM system.....14
2.14 Competitive assay for studying small molecules binding affinity.....14
3. Glycoprotein polarization in chemotaxis.....15
3.1 A chemotaxis example.....15
3.2 Chemoattractant concentration gradient generated by a micropipette.....15
3.3 Analysis of average glycoprotein density increase in the leading edge during chemotaxis.....16
4. Mapping nicotinic acetylcholine receptors (nAChR).....17
4.1 Influence of non-specific immunoglobulins - negative control.....17
4.2 Immunofluorescence control experiments.....18

1. Flow system

A drug perfusion system[1] was used to rapidly deliver sample solutions with well-defined concentrations to interact with the cells on the SPR chip. As shown in Fig. S1, two valves were used to switch the flow between sample and buffer channels. Depending on the positions of the valves, either the buffer or sample solution is delivered to the cells via a tube closely placed (50 µm) over the target cells with the help of a micromanipulator. Note that the inner diameter of the tube is 450 µm, which is much larger than a cell (20-50 µm), so that the sample or buffer flow can completely cover the target cells and surrounding spaces. Fig. S1c shows the SPR time profile recorded during the injection of a 50 mM GlcNAc solution. The transition time is as fast as ~1 second, and the concentration from the SPR signal matches 50 mM, indicating no dilution effect.

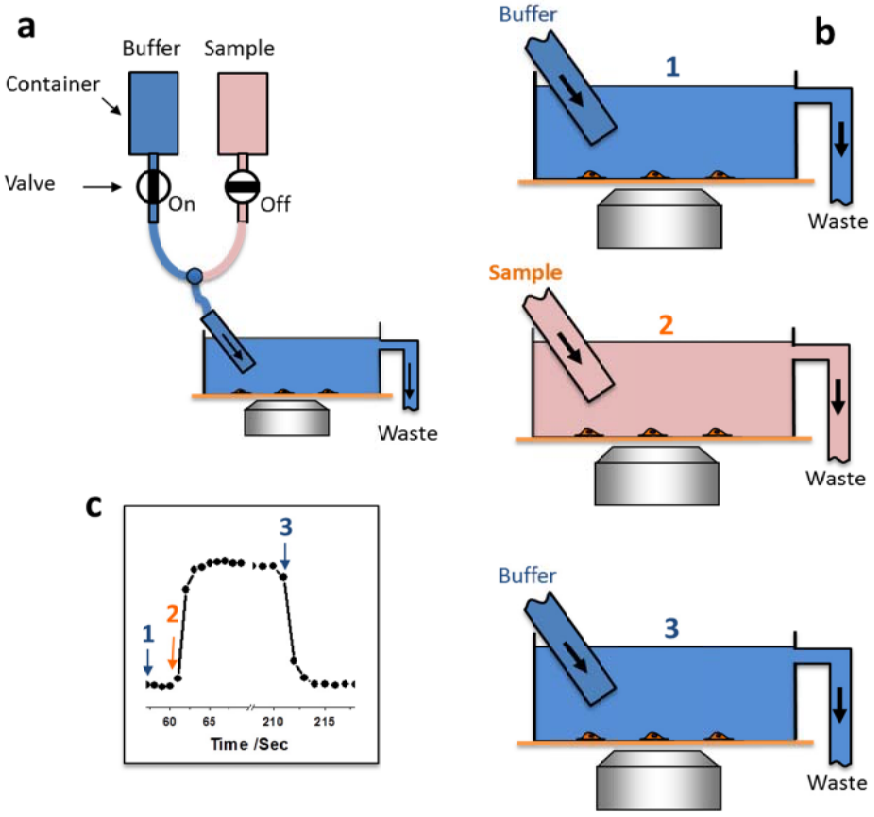

Fig. S1. (a) Flow system for rapid delivery of sample and buffer solutions. (b) Operation of the flow system. Initially, the buffer valve is open and the sample valve is closed, so that the target cells is covered by 100% buffer (b1). When injection of the sample solution is needed, the buffer

valve is closed the sample valve is open, which exposes the target cells with 100% sample solution (b2), allowing study of association processes. Finally, to study dissociation processes, the sample valve is closed and the buffer valve is re-open. (c) Performance of the flow system. To examine the effectiveness of the flow system, we tested a 50 mM sugar solution. The SPR profile shows that the transition time from one solution to another is as fast as ~ 1 second and the corresponding SPR response matches the 50 mM concentration, indicating no dilution effect. The flow rate can be controlled by the height of the container (gravity), however the typical flow rate was 350 µL/min in the present work.

2. Glycoprotein-lectin interaction

2.1 SPRM movie and corresponding snapshots

An appropriate way to illustrate the local binding activities across the cell surface is via a movie (e.g., Movie S1). Note that the background SPRM image was subtracted from all the frames in Movie S1 in order to demonstrate the SPR signal changes due to the WGA binding. Figs. S2a-d show 4 snapshots from Movie S1 during the binding experiment shown in Fig. S2e. Fig. S2d also demonstrates the effectiveness of the surface regeneration by GlcNAc.

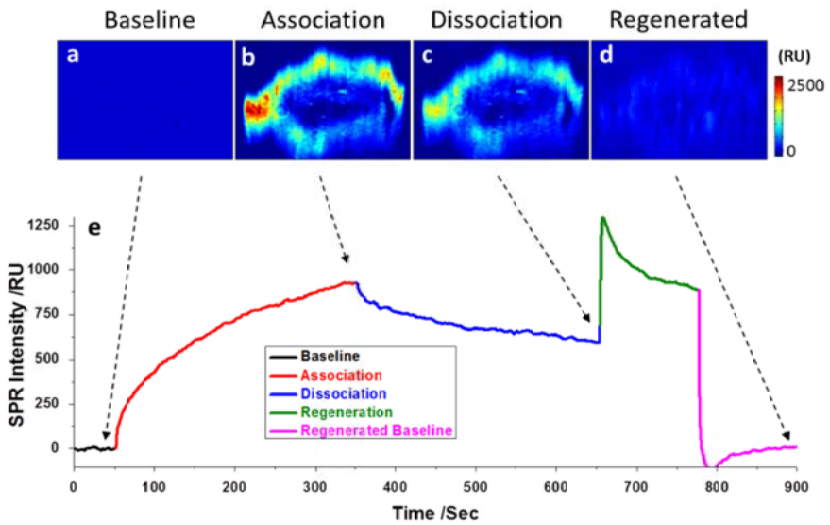

Fig. S2. (a-d). Typical snapshots extracted from Movie S1. (e). Averaged SPR sensorgram over a

whole cell. The dashed arrows mark the moments at which the snapshots were taken.

2.2 The inhibition effect of N-acetyl glucosamine (GlcNAc)

The inhibition effect of GlcNAc on wheat germ agglutinin (WGA) binding was examined in order to better understand the SPR signal increase after the WGA injection. The red curve in Fig. S3 is a sensorgram recorded when an 80 µg/mL WGA solution was flowed over an adhered cell. When the same 80 µg/mL WGA solution was mixed with 50 mM GlcNAc and incubated for 10 mins before flowing over the same cell, no binding signals was observed, as shown in Fig. S3 (black curve). This experiment demonstrated that WGA does not interact with the GlcNAc-containing glycoproteins in the cell membrane if they are bound to GlcNAc in the solution. This observation supports that the interaction between WGA and GlcNAc groups in glycoproteins was the reason for the observed SPR increase after WGA injection. Note that the jump in the black curve during the association period was due to the bulk refractive index change from the 50 mM GlcNAc solution, which has a high mass concentration of 11 mg/mL. The red curve does not show any bulk effect because the mass concentration of WGA was low (80 µg/mL).

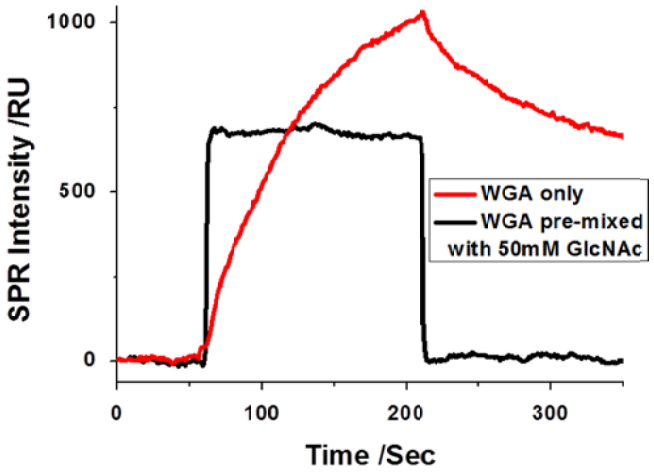

Fig. S3. SPR sensorgrams of a cell by flowing 80 µg/mL WGA solution only (red curve) and 80 µg/mL WGA solution pre-mixed with 11 mg/mL (50mM) GlcNAc (black curve), respectively.

2.3 Repeatable regeneration of cell surface

Fig. S4 shows that repeatable SPR sensorgrams can be obtained by flowing 50 mM GlcNAc solution over a WGA-bound cell surface for 60 seconds and followed by regeneration of the binding sites on the cell surface. The result also demonstrates that the surface regeneration with GlcNAc is highly effective without affecting the binding sites of the cell.

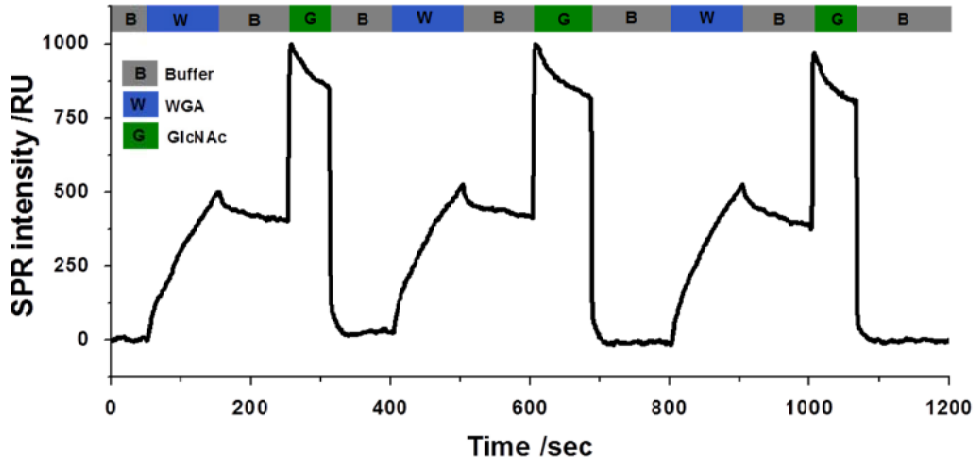

Fig. S4. Repeatable binding-and-regeneration of a fixed cell by sequentially flowing buffer, WGA (sample) and GlcNAc (regeneration) solutions over the cell.

2.4 Interaction between WGA and poly-L-lysine

WGA interaction with poly-L-lysine coated gold surface without cell culture process was studied in order to evaluate the influence of poly-L-lysine modification on WGA binding. The SPR signal is ~50 RU (Fig. S5), which is much smaller than ~600 RU SPR response for WGA binding onto the cell.

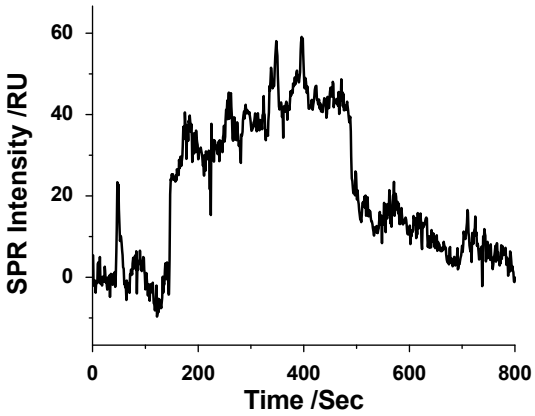

Fig. S5. Interaction of WGA with poly-L-lysine without cell attachment.

2.5 Multiple cell responses

The SPRM images of multiple cells were recorded simultaneously during a WGA binding experiment in order to demonstrate that a) the observed change in SPR signals is a general phenomenon for all the cells and b) the amount of bound WGA varies from cell to cell. By increasing the view area of the SPRM system, the bright field and SPRM images can image 7 cells (Figs. S6a and S6b). The SPR sensorgrams of individual cells as marked by colored polygons in Fig. S6b can be analyzed and the findings are shown in Fig. S6c. WGA association and dissociation take places in all the cells, but the amount of binding varies from cell to cell, reflecting different abundance levels of GlcNAc-containing glycoproteins on different cells. Data analysis on the maximal SPR signal showed the average response was 1415 RU with a standard derivation of 194 RU. The relative standard derivation was 14%.

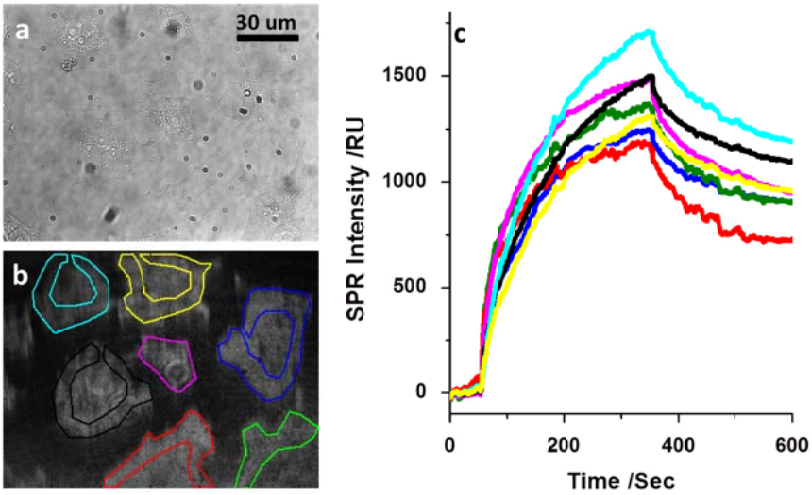

Fig. S6. Bright field (a) and SPRM (b) images of multiple SH-EP1 cells. The SPR sensorgrams (c) of the individual cells obtained by analyzing the SPR intensity over the edge region of each cell as indicated by the colorful polygon in (b).

2.6 Influence of cell fixation on the binding kinetics

We compared the SPR responses in the same cells when they were alive and fixed. We found that the cells in the living and fixed states have similar binding kinetics but different amounts of binding (Fig. S7). The smaller amount of binding when the cells were could be attributed to the damage to the binding site during fixation. The fitted associate and dissociate rate constants for live and fixed cells are listed in Table S1. No significant difference in the association rate constant (ka) was found. However, the dissociation rate constant of the live cell was about one half of that of the fixed cells, indicating a slower dissociation when cells were alive. Such results might be related with the WGA uptake by live cells through a receptor mediated endocytosis, which was eliminated for the fixed cells. [2]

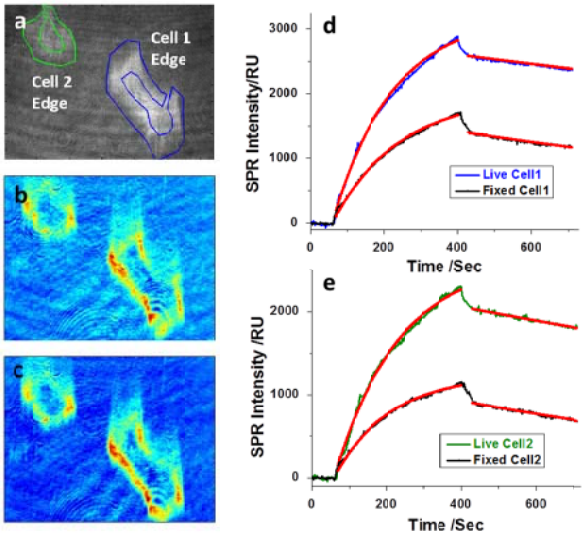

Fig. S7. (a) SPR image of two live cells. (b) The SPRM increase after the WGA binding to the cells before (b) and after (c) fixation show similar spatial features, indicating the fixation treatment did not significantly affect the distribution of the WGA binding sites. The SPR sensorgrams in Cell 1 and Cell 2 edge regions as indicated in (a) are displayed in (d) and (e), respectively, where the blue and black curves are for the live and fixed cells, respectively. The red curves show the curve fitting results on the basis of a first order kinetics model.

Table S1. Fitted association and dissociation rate constants for live and fixed cell.

		k_a (M^{-1} s^{-1})	k_d (s^{-1})	K_D (nM)
Cell1	Live	4.5×10^{3}	2.9×10^{-4}	64
	Fixed	3.7×10^{3}	6.3×10^{-4}	170
Cell2	Live	4.0×10^{3}	4.3×10^{-4}	110
	Fixed	4.3×10^{3}	9.6×10^{-4}	220

2.7 Flow rate

Two different flow rates (350 and 200 μL/min) were tested and no significant difference in the association and dissociation rate constants was observed (Fig. S8), demonstrating that mass transport effect is small in the experiments.

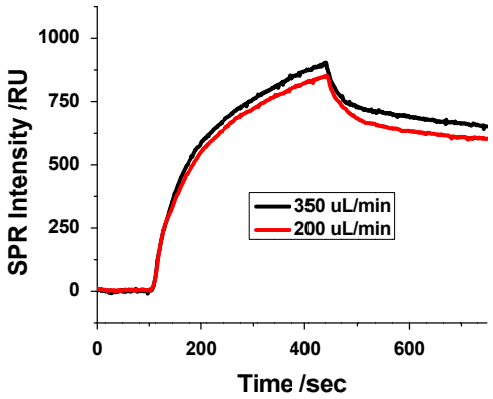

Fig. S8. SPR sensorgrams for the same cell obtained at different flow rates (350 µL/min, black curve, and 200 µL/min, red curve).

2.8 Long recording time

The dissociation was recorded for 40 minutes to obtain a comprehensive understanding to the binding kinetics. The recorded dissociation curve showed a fast and then followed with a slow dissociation process, as shown in Fig. S9(a). Such feature was consistent with the previous publications in which two-stage dissociation was also observed.[3] In the present work, a dissociation time of 5 minutes was selected in order to avoid the system drift that might occur during recording, as shown in Fig. S9(b).

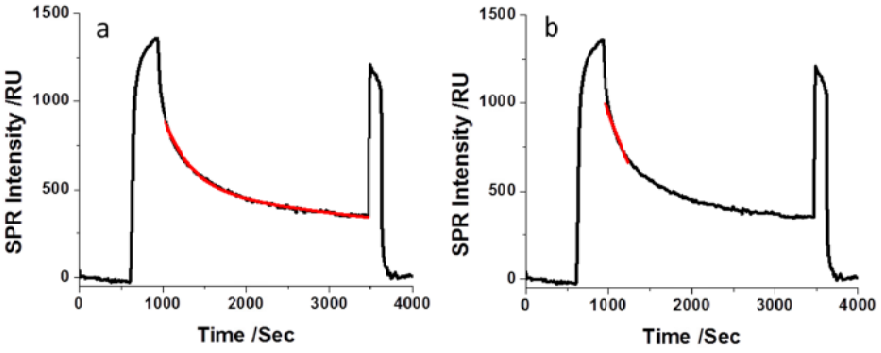

Fig. S9. SPR sensorgrams and the corresponding curve fitting over 1 hour recording period. The dissociation process can be fit with two exponential decays leading to rate constants of 3.0×10^{-3} and 1.5×10^{-4} s^{-1}, respectively (a). The dissociation rate constant was determined to be 1.9×10^{-3} s^{-1} if one-factor fitting was applied to the SPR data in the initial five minutes (b).

2.9 Receptor density estimation

The WGA binding site density was estimated to be 3.8×10^4 per μm^2 from the SPR response (~1200 RU). This density corresponds to 27 nm^2 per sugar unit, which is not dense considering the small size of a sugar molecule (~1 nm). This estimation used a conversion factor that 1 pg/mm^2 protein gives 0.5 RU SPR response. It is generally accepted that a protein density of 1 pg/mm^2 leads to 1 RU if the protein binding takes place close to the sensor surface.[4] In the present work, the binding takes place on cell surfaces, which are 50-100 nm away from the gold film.[5] At these distances, the SPR sensitivity drops by ~50% based on simulation using WinSpall developed by Dr. Wolfgang Knoll[6] (Fig. S10). For this reason, we assumed that 1 pg/mm^2 corresponds to 0.5 RU SPR response units for a crude estimate of the protein coverage.

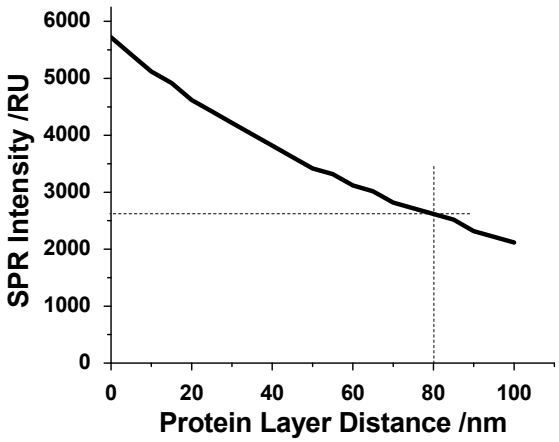

Fig. S10. SPR response caused by the binding of a protein monolayer (refractive Index = 1.5) in PBS buffer at different distances from the sensor surface.

2.10 Association and dissociation constant maps

Two data processing strategies were applied to obtain the association and dissociation rate constant maps (Figs. 3b and 3c). The first strategy was to use a 15-point two dimensional-filter (similar to pixel binning) to remove pixel-to-pixel noises in the SPRM

images. The second one was a global fitting strategy to fit the binding kinetic curves at different concentrations. The latter strategy is particularly useful when the dissociation rate is low and data recording period is short. It also helps when the noise level from the individual pixels is high. In the present work, we fit the association curves at 4 different WGA concentrations (varying from 10 to 200 μg/mL), from which we determined the fitting parameter, k_{obs}, at each concentration. k_{obs} is related to the association and dissociation rate constants, k_a and k_d by $k_{obs}=k_a*C_{WGA}+k_d$, where C_{WGA} is WGA concentration. We then used a linear regression to obtain k_a and k_d (from the slope and intercept of the linear regression). Note that only the locations with a good fitting quality (correlation coefficient >= 0.9) were shown. The k_a and k_d values at regions with poor fitting quality (correlation coefficient < 0.9) due to noisy data were set to be zero. An example of such regions is the central part of the cell.

2.11 Equilibrium dissociation constant analysis

We obtained the equilibrium responses at different WGA concentrations and plotted in Fig. S11a. The binding affinity resolved from the equilibrium responses was 0.32 μM. It is well consistent with the K_D value resolved from the kinetics analysis (0.23 μM) based on a global fitting. Note that since the SPR response did not reach full steady state (equilibrium) at low concentrations within the five minutes recording window, curve fitting method described in Section 2.10 was applied to estimate the corresponding equilibrium response (see Fig. S11b). The equilibrium plot shown in Fig. S11a follows the Langmuir isotherm.

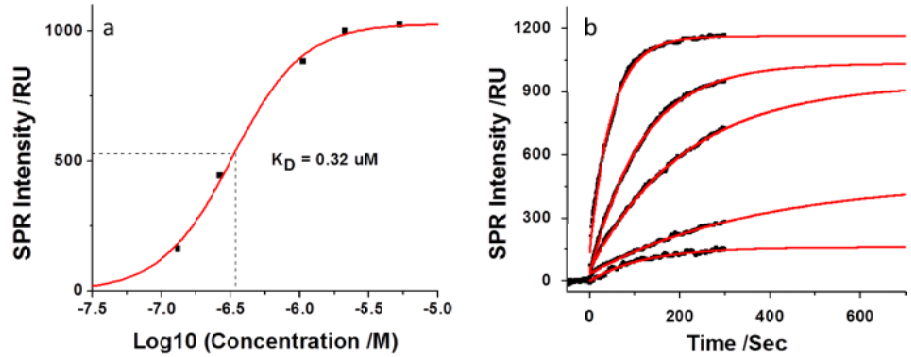

Fig. S11. (a) Binding affinity (K_D) was determined to be 0.32 μM from the equilibrium analysis. (b) The equilibrium signals were obtained by fitting the association curves in the initial 5 mins.

2.12 Spatial variation of dissociation rate constant (k_d) in Fig. 3c.

In order to quantitatively analyze the spatial variation of dissociation rate constant (k_d) in Fig. 3c, a histogram of k_d from different pixels (Fig. S12a) was created and shown in Fig. S12b. The measured dissociation rate constant follows a Gaussian distribution with a well-defined peak at 5×10^{-3} s^{-1} and a relatively small standard deviation of 2×10^{-3} s^{-1}. The analysis indicates that despite the observed spatial variability in the rate constant afforded by our SPRM approach, most regions have the rate constants close to the average value.

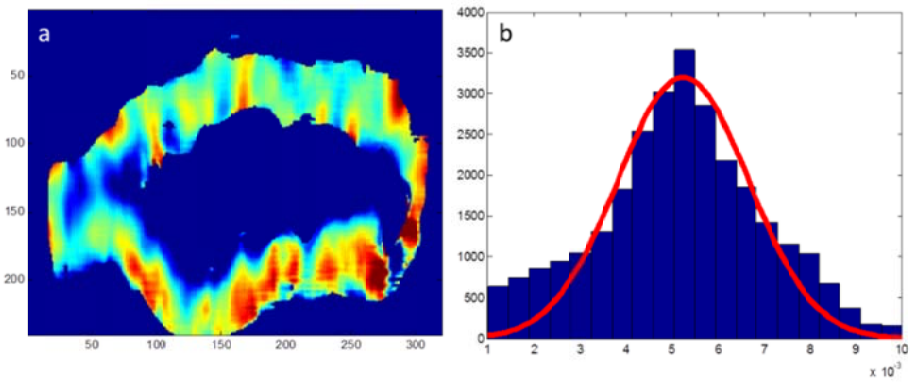

Fig. S12. Dissociation rate constant (k_d) map (a) and the histogram of the spatial variability (b) of k_d. The red curve shown in (b) is a Gaussian fit.

2.13 Sensitivity of the present SPRM system

The noise level of the present setup is ~10 RU on a single cell level, corresponding to ~80 antibody binding sites per μm^2. This detection limit is adequate for many applications. For example, for an expression level 1 million receptors per cell,[7] the receptor density is ~800 receptors per μm^2 if assuming a cell diameter of 20 μm, which can be easily detected. Further, because of heterogeneous distribution of receptors, the local receptor density can be substantially higher than the average value, making it easier to detect with SPRM.[8]

The detection limit of the current set up can be further improved. Commercial SPR can achieve a detection limit as small as 0.1 RU. We have identified that the light source is the major source of noises, and the CCD camera as the second source when single pixel analysis is needed. We have been seeking to purchase new light source with proper temperature control and new CCD camera to further improve the system performance.

2.14 Competitive assay for studying small molecules binding affinity

We carried out preliminary experiments to address the potential of our method for studying the binding of small molecules to membrane proteins using competitive assay. In our experiments, GlcNAc (a small molecule) at different concentrations was introduced to competitively bind to WGA (large protein ligand) pre-bound onto the membrane receptors of a cell. As shown in Fig. S13, the initial binding of WGA onto the cell surface led to a rise in the SPR intensity, the dissociation caused by the introduction of GlcNAc resulted in a decrease in the SPR intensity. The dissociation rate increases with GlcNAc concentration, which is expected for competitive assay. Note that GlcNAc is not a drug candidate, but the experiments demonstrate a capability of studying small molecules via competitive assay on single cell level, which is anticipated to be useful for screening small molecule drugs.

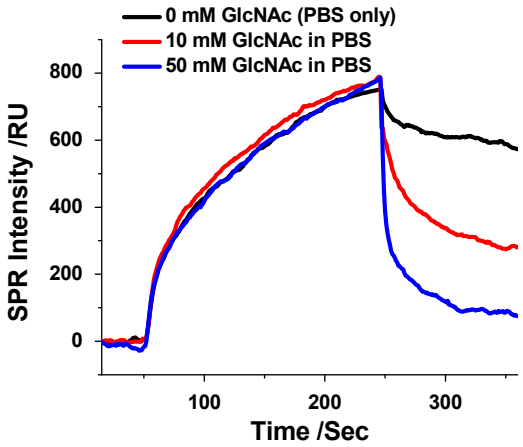

Fig. S13. Dissociation of WGA from a cell surface due to competitive binding of GlcNAc at different concentrations (0 mM - black curve, 10 mM - red curve and 50 mM – blue curve).

3. Glycoprotein polarization in chemotaxis

3.1 A chemotaxis example

Movie S2 shows continuously recorded SPRM images of a single adhered SH-EP1 cell during a chemotaxis process. A pipette tip filled with fetal bovine serum (FBS) was located in the left side of the view. The target cell slowly migrated towards the pipette tip in a recording time of 3.3 hours. The size of the view is 80 × 60 μm (horizontal × vertical).

3.2 Chemoattractant concentration gradient generated by a micropipette

A micropipette tip filled with chemoattractant is one of the widely used strategies to create a concentration gradient in the chemotaxis studies.[9] In order to estimate the generated concentration gradient, a COMSOL model was established to simulate the concentration distribution caused by a static diffusion in 20 mins in a container with the diameter of 10 mm, which matched the experimental conditions. The diffusion coefficient of protein in the buffer solution was set to be $5x10^{-11}$ m^2/s based on the reported value in literature.[10] It was found that the concentration difference was about

10% between the leading edge and the opposite edge for a 40-μm size adherent cell. This concentration gradient as shown in literature is sufficient to induce cell movement.[9]

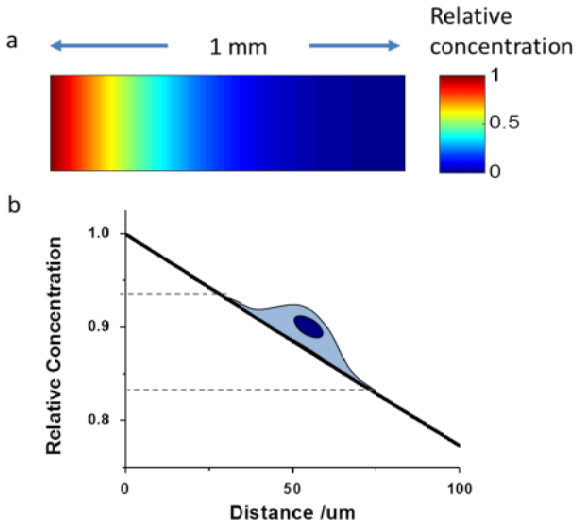

Fig. S14. (a) The peusdo-color map of the relative concentration distribution after a static diffusion of 20 minutes in a 10 mm size container. (b) The concentration profile in the first 100 μm, which corresponds to ~10% concentration difference between the leading and rear edges of a cell (typical size of 40 μm).

3.3 Analysis of average glycoprotein density increase in the leading edge during chemotaxis

The average glycoprotein density in the leading edge before and after the chemotaxis was analyzed by calculating the average SPR increase in the selected region as shown in Figs. S15. The average SPR increase was estimated to be 720 and 920 RU, respectively, indicating a 28% increase in the glycoprotein density in the leading edge.

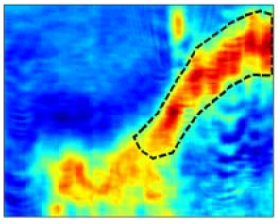

Fig. S15. Selected region in the leading edge for calculation of average glycoprotein density.

4. Mapping nicotinic acetylcholine receptors (nAChR)

4.1 Influence of non-specific immunoglobulins - negative control

In order to investigate possible influence of non-specific immunoglobulins in the antibody solution, fixed cells were incubated with normal rat serum for 1 hour before the experiments. Fig. S16 (red curve) shows the SPR sensorgram of anti-nAChR alpha4 antibody when flowing through the engineered SH-EP1 cells. The red curve represents the average response of seven cells, while the pink background represents the standard derivation. The similar bulk effect as well as specific antibody association and dissociation features were observed, indicating the interactions between the nAChRs expressing cell surface and the antibody solution took place. Moreover, isotype rat IgG solution also flowed over the same seven cells as a negative control (black curve). The SPR sensorgram displays a typical bulk effect feature, implying that the interactions observed in the red curve was not from the non-specific interaction between cells and the normal rat IgG. Such bulk effect was due to the difference in refractive index between the antibody solution and the running buffer.

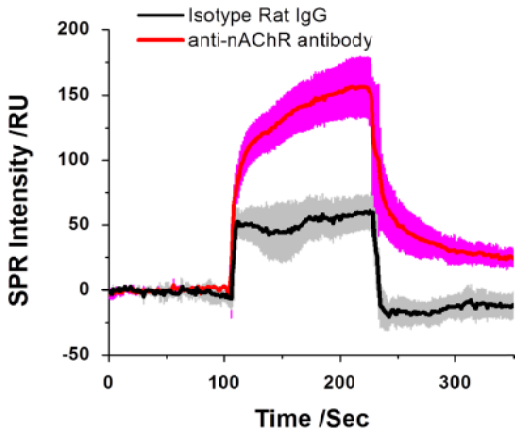

Fig. S16 SPR sensorgrams of seven engineered SH-EP1 cells when flowing anti-nAChRs alpha4 antibody (red curve) and isotype rat IgG (black curve) solutions. The red and black curves are the average responses of the seven cells, and the pink and grey plots show the standard derivations of the seven measurements.

4.2 Immunofluorescence control experiments

Control experiments were performed to validate the quality of immunofluorescence measurements. The engineered cells incubated with primary and secondary antibody served as positive controls. As an example, bright field and immunofluorescence images of a cell are shown in Figs. S17a and S17d. Similar studies were carried out on a wildtype cell that did not express nAChR in its cell membrane as a negative control, and the corresponding immunofluorescence image did not show any fluorescence signal (Fig. S17e), indicating no binding took place. Another negative control carried out was to incubate the secondary antibody with the engineered cells in the absence of primary antibody. Again in this case, no fluorescence was detected (Fig. S17f). The lack of background fluorescence in Figs. S17e and f was mainly due to the presence of 47-nm gold film, which greatly decreased the fluorescence emission via both quenching and light absorption. These control experiments confirmed that (1) nAChR was expressed in the engineered cells and (2) the immunofluorescence measurements worked properly.

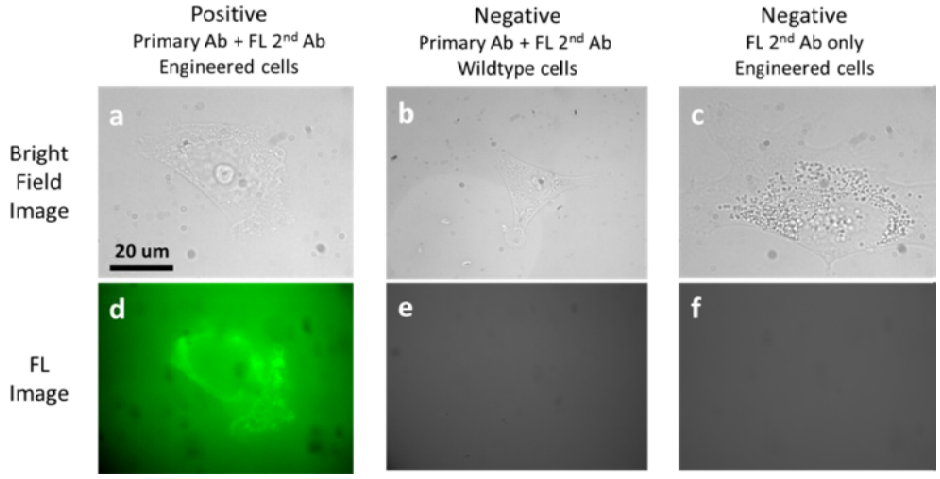

Fig. S17. Typical bright field (a-c) and immunofluorescence (d-f) images of three immunofluorescence control measurements. Positive control was performed by sequentially incubating primary and secondary antibodies with engineered cells. First negative control followed the same procedure to wildtype cells. Second negative control was performed by incubating secondary antibody with engineered cells only.

References:

1. Osorio, N. & Delmas, P. Patch clamp recording from enteric neurons in situ. *Nature Protocols* **6**, 15 (2011).

2. Liu SL *et al.* Visualizing the endocytic and exocytic processes of wheat germ agglutinin by quantum dot-based single-particle tracking. *Biomaterials* **32**, 7616 (2011).

3. Vila-Perello, M., Gallego, R.G. & Andreu, D. A simple approach to well-defined sugar-coated surfaces for interaction studies. *ChemBioChem* **6**, 1831 (2005).

4. BIACORE AB, BIAtechnology Handbook, Uppsala, Sweden. (1998).

5. Iwanaga, Y. Cell-substrate distance measurement in correlation with distribution of adhesion molecules by fluorescence microscopy. **Technische Universität München** (2000).

6. http://www.mpip-mainz.mpg.de/groups/knoll/software.

7. DeFazio-Eli, L. *et al.* Quantitative assays for the measurement of HER1-HER2 heterodimerization and phosphorylation in cell lines and breast tumors: applications for diagnostics and targeted drug mechanism of action. *Breast Cancer Res.* **13**, R44 (2011).

8. Manz, B.N. & Groves, J.T. Spatial organization and signal transduction at intercellular junctions. *Nature Rev. Mol. Cell Biol.* **11**, 342 (2010).

9. Insall, R.H. Understanding eukaryotic chemotaxis: a pseudopod-centred view. *Nature Rev. Mol. Cell Biol.* **11**, 453 (2010).

10. Biophysics of DNA-protein Interactions: From Single Molecules to Biological Systems, by Mark C. Williams, 1st Edition, Springer 2011, Page 50.